Supplemental information

scCURE identifies cell types responding

to immunotherapy and enables outcome prediction

Xin Zou, Yujun Liu, Miaochen Wang, Jiawei Zou, Yi Shi, Xianbin Su, Juan Xu, Henry H.Y. Tong, Yuan Ji, Lv Gui, and Jie Hao
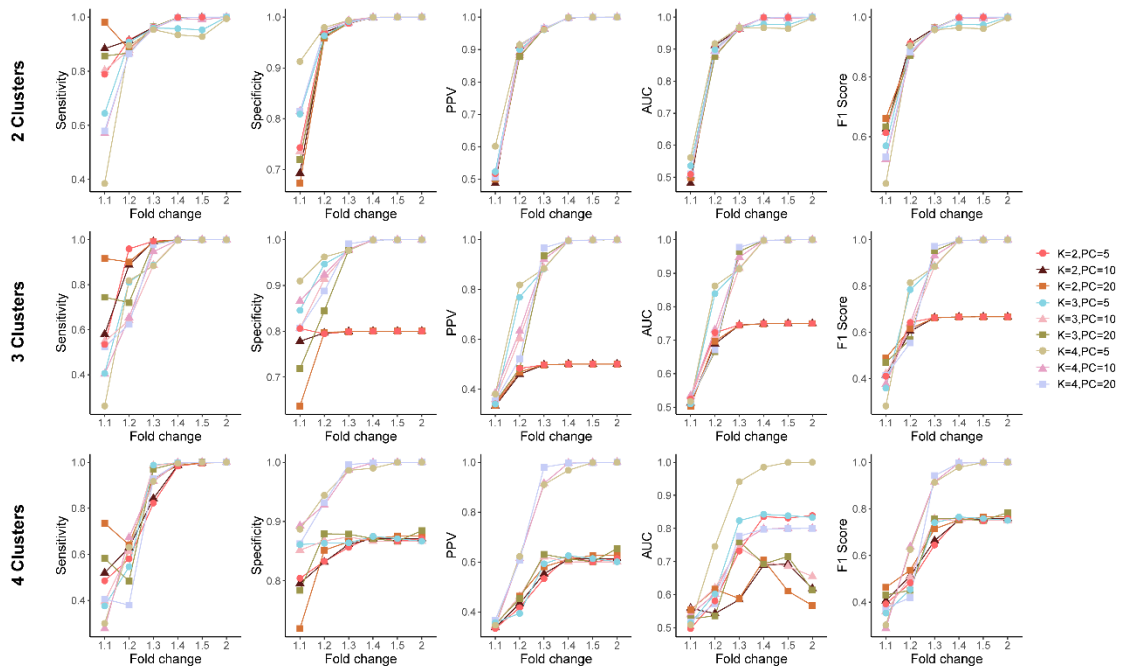
Supplemental information

scCURE integrates cancer immunotherapy outcome prediction and mechanism interpretation by recognizing changed and unchanged cells during treatment

Xin Zou, Yujun Liu, Miaochen Wang, Jiawei Zou, Yi Shi, Xianbin Su, Juan Xu, Henry H. Y. Tong, Yuan Ji, Lv Gui, Jie Hao
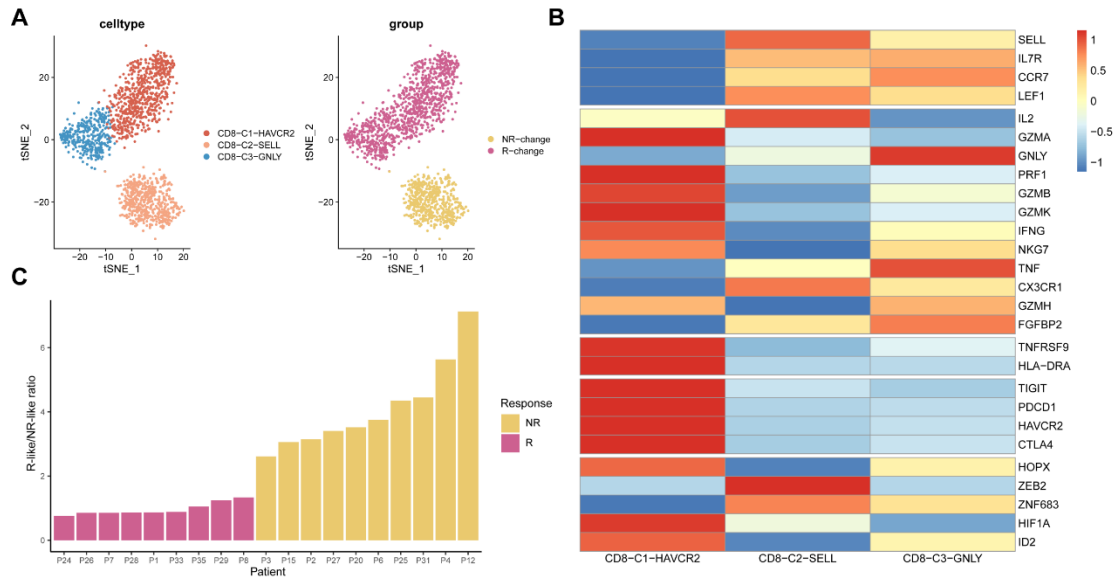

Figure S1. scCURE evaluation of simulated data in different numbers of principal components, related to Figure 2. The values of K and PC for pre- and post-treatment cells were set to equal.

14

15 **Figure S2. scCURE identified predictive R-change and NR-change CD8+ T cells from pre-**

16 **treatment melanoma patients, related to Figure 3.** (A) t-SNE plot of the scCURE processed CD8+

17 T cells colored by cell type, cell group and ICB response. (B) Heatmap of canonical CD8+ T cell

18 functional markers. (C) Barplot showing the well distribution of R-change/NR-change ratios

19 between responders and non-responders. For the cells simultaneously identified as changed ones

20 when comparing pre-treatment to post-treatment responders and non-responders, respectively, those

21 cells will be excluded from the ratio calculation.

22
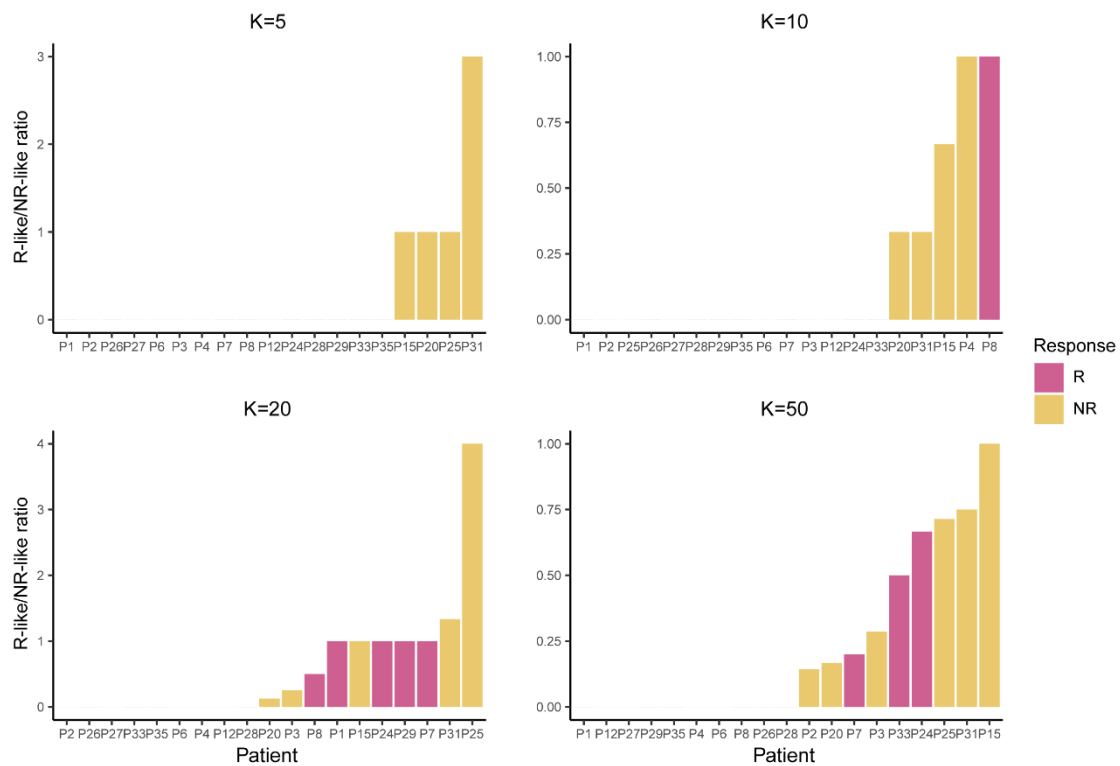
**Figure S3. Histogram of the R-like/NR-like ratios at different K values by MNN method between responders and non-responders, related to Figure 3.** The R-like/NR-like ratios for each patient were distributed on the barplot.
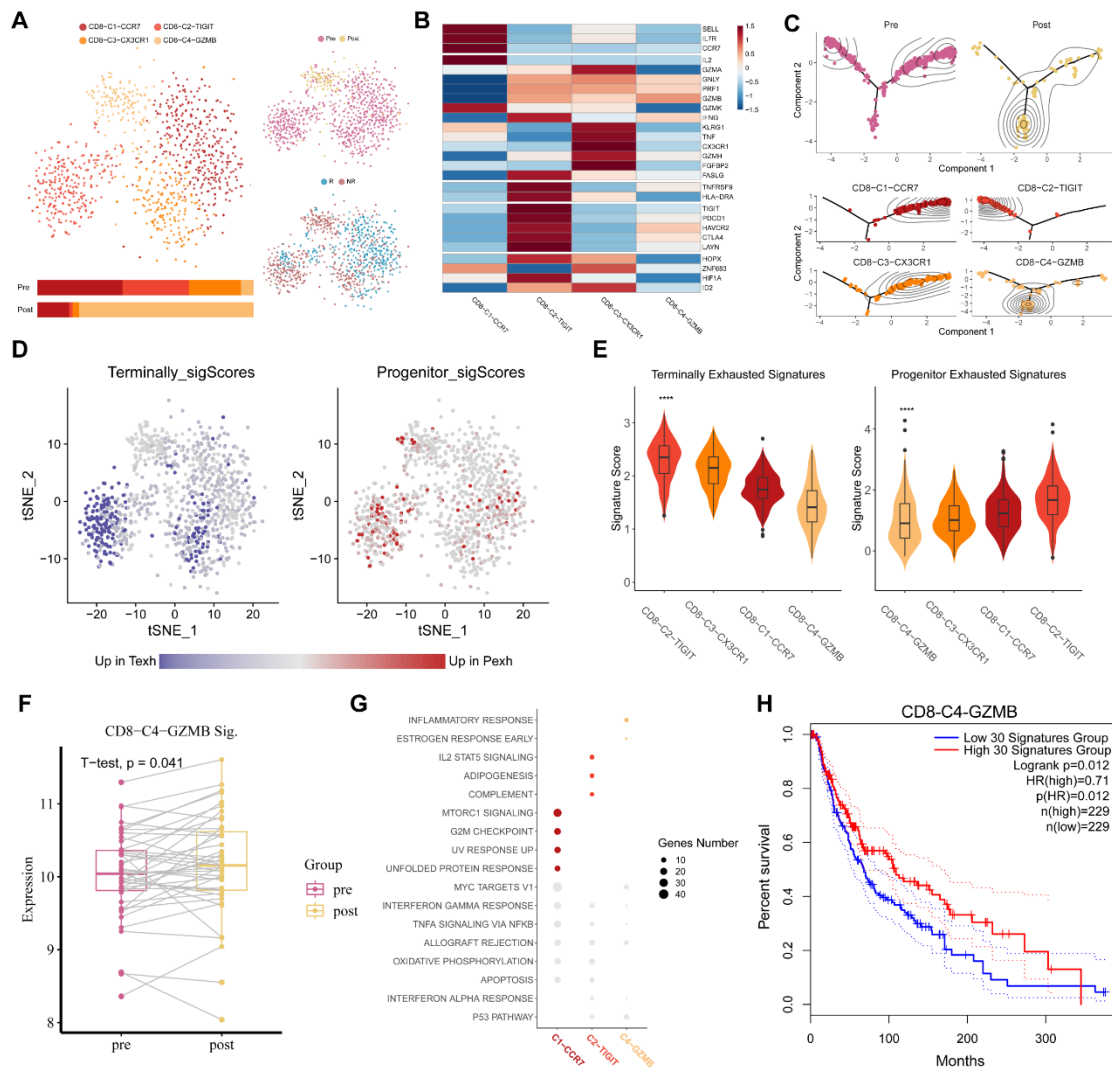
Figure S4. The ICB treatment response mechanism explained in the scCURE identified changed CD8$^+$ T cells between pretreatment samples and posttreatment nonresponders, related to Figure 4. (A) Heterogeneity of the dynamical CD8$^+$ T cells shown in the t-SNE scatter plot. Cell cluster frequency shown as a fraction of total cells in pretreatment and posttreatment. (B) Heatmap shows the expression of canonical T cell functional markers across cell clusters. (C) Pseudotime trajectory reconstruction and its association with cell clusters and sample labels. (D) Heatmap in t-SNE space showing the signature scores for terminally exhausted and progenitor exhausted CD8$^+$ T cells. (E) Terminally exhausted and progenitor exhausted CD8$^+$ T cell signatures across CD8$^+$ T cell subtypes. (F) Signature scores for the top 30 markers of CD8-C4-GZMB in bulk RNA-seq samples from the GSE91061 melanoma cohort. (G) Enriched GSEA hallmarks of two representative CD8$^+$ T clusters of pre- and posttreatment samples. (H) Survival analysis using the top 30 markers of CD8-C5-IL7R on TCGA melanoma data.
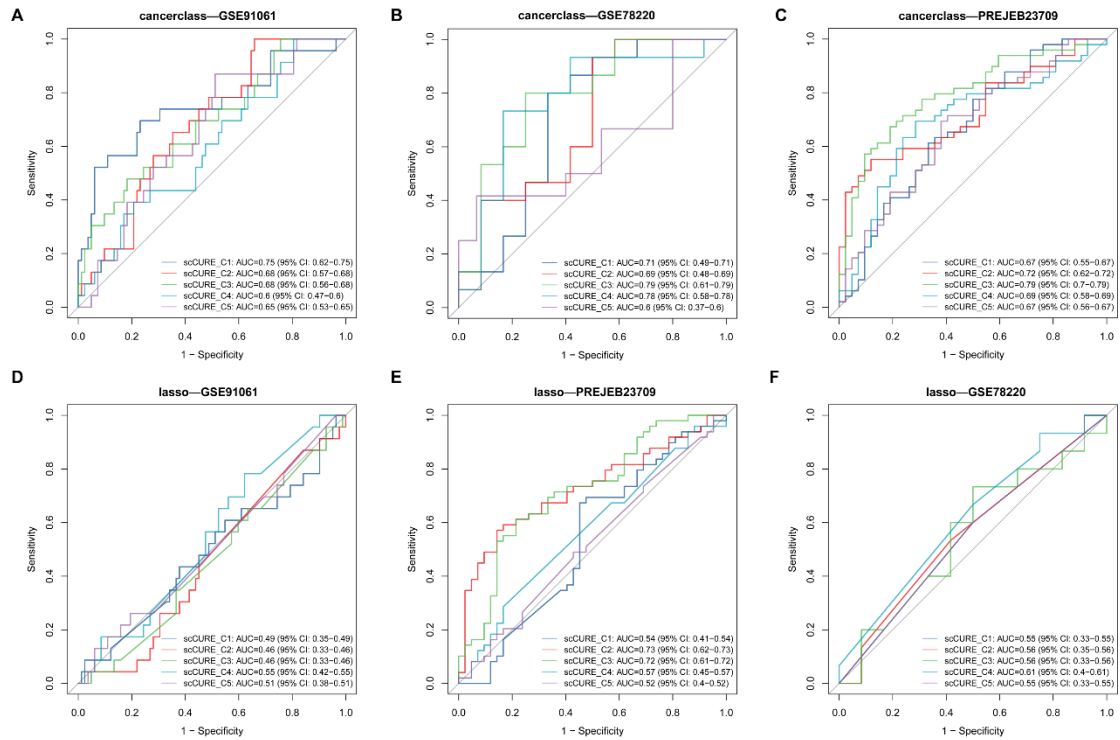
**Figure S5. The evaluation of predictive performance of each cluster by different machine learning methods in three independent bulk melanoma cohorts, related to Figure 5.** (A, B, C) The multiple ROC plot depicting the predictive performance of each cluster using cancerclass in three independent cohorts. (D, E, F) The multiple ROC plot depicting the predictive performance of each cluster using lasso in three independent cohorts.
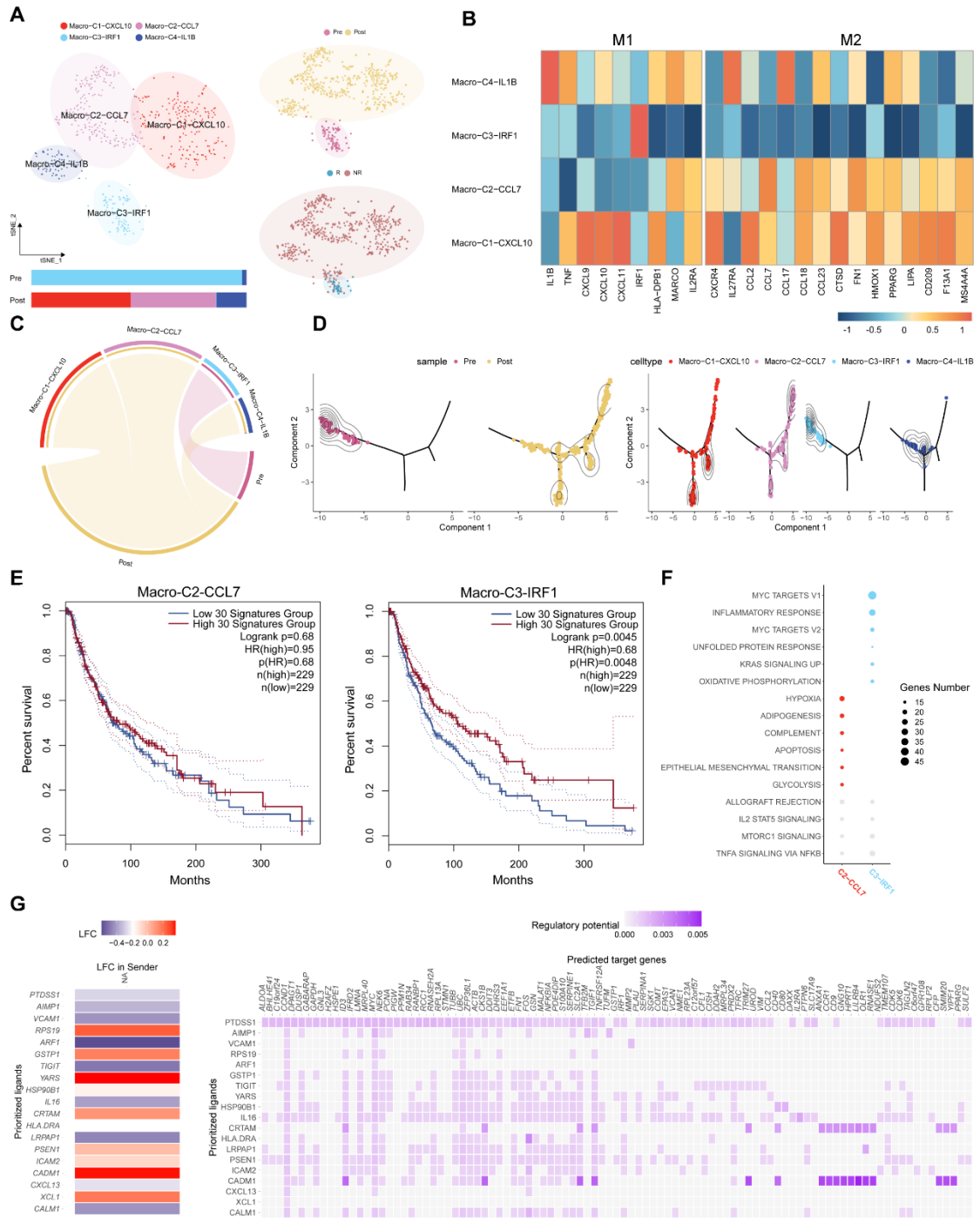
Figure S6. Macrophage cell dynamics in nonresponders, related to Figure 6. (A) Heterogeneity of the dynamical macrophage cells shown in the t-SNE scatter plot. Cell cluster frequency shown as a fraction of total cells in pretreatment and posttreatment. (B) Heatmap showing the signature scores for M1 and M2 macrophages. (C) Enrichment of different cell clusters in pre- and post-samples. (D) Pseudotime trajectory reconstruction and its association with cell clusters and sample labels. (E) Survival analysis using the top 30 markers of C2-CCL7 and C3-IRF1. (F) Enriched GSEA hallmarks of two representative macrophage clusters of pre- and posttreatment samples. (G) Cell-cell communication between macrophages and CD8^{+} T cells in non--responders.